Inorganic Chemistry

Article

pubs.acs.org/IC

Bifunctional $Zn^{II}Ln^{III}$ Dinuclear Complexes Combining Field Induced SMM Behavior and Luminescence: Enhanced NIR Lanthanide Emission by 9-Anthracene Carboxylate Bridging Ligands

María A. Palacios,[†] Silvia Titos-Padilla,[†] José Ruiz,[†] Juan Manuel Herrera,*[,†] Simon J. A. Pope,[‡] Euan K. Brechin,[§] and Enrique Colacio*[,†]

[†]Departamento de Química Inorgánica, Facultad de Ciencias, Universidad de Granada, Avda. Fuentenueva s/n, 18071 Granada, Spain

[‡]Cardiff School of Chemistry, Cardiff University, Park Place, Cardiff CF10 3AT, United Kingdom

[§]EaStCHEM School of Chemistry, The University of Edinburgh, West Mains Road, Edinburgh EH9 3JJ, United Kingdom

Supporting Information

ABSTRACT: There were new dinuclear Zn^{II}–Ln^{III} complexes of general formulas $[Zn(\mu\text{-L})(\mu\text{-OAc})Ln(NO_3)_2]$ (Ln^{III} = Tb (**1**), Dy (**2**), Er (**3**), and Yb (**4**)), $[Zn(\mu\text{-L})(\mu\text{-NO}_3)Er(NO_3)_2]$ (**5**), $[Zn(H_2O)(\mu\text{-L})Nd(NO_3)_3]\cdot 2CH_3OH$ (**6**), $[Zn(\mu\text{-L})(\mu\text{-9-An})Ln(NO_3)_2]\cdot 2CH_3CN$ (Ln^{III} = Tb (**7**), Dy (**8**), Er (**9**), Yb(**10**)), $[Zn(\mu\text{-L})(\mu\text{-9-An})Yb(9\text{-An})(NO_3)_3]\cdot 3CH_3CN$ (**11**), $[Zn(\mu\text{-L})(\mu\text{-9-An})Nd(9\text{-An})(NO_3)_3]\cdot 2CH_3CN\cdot 3H_2O$ (**12**), and $[Zn(\mu\text{-L})(\mu\text{-9-An})Nd(CH_3OH)_2(NO_3)]\text{-}ClO_4\cdot 2CH_3OH$ (**13**) prepared from the reaction of the compartmental ligand *N,N′,N″*-trimethyl-*N,N″*-bis(2-hydroxy-3-methoxy-5-methylbenzyl)diethylenetriamine (H_2L), with $ZnX_2\cdot nH_2O$ (X = NO_3^- or OAc^-) salts, $Ln(NO_3)_3\cdot nH_2O$, and, in some instances, 9-anthracenecarboxylate anion (9-An). In all these complexes, the Zn^{II} ions invariably occupy the internal N_3O_2 site whereas the Ln^{III} ions show preference for the O_4 external site, giving rise to a $Zn(\mu$-diphenoxo)Ln bridging fragment. Depending on the Zn^{II} salt and solvent used in the reaction, a third bridge can connect the Zn^{II} and Ln^{III} metal ions, giving rise to triple-bridged diphenoxoacetate in complexes **1**–**4**, diphenoxonitrate in complex **5**, and diphenoxo(9-anthracenecarboxylate) in complexes **8**–**13**. Dy^{III} and Er^{III} complexes **2**, **8** and **3**, **5**, respectively, exhibit field induced single molecule magnet (SMM) behavior, with U_{eff} values ranging from 11.7 (3) to 41(2) K. Additionally, the solid-state photophysical properties of these complexes are presented showing that ligand L^{2-} is able to sensitize Tb^{III}- and Dy^{III}-based luminescence in the visible region through an energy transfer process (antenna effect). The efficiency of this process is much lower when NIR emitters such as Er^{III}, Nd^{III}, and Yb^{III} are considered. When the luminophore 9-anthracene carboxylate is incorporated into these complexes, the NIR luminescence is enhanced which proves the efficiency of this bridging ligand to act as antenna group. Complexes **2**, **3**, **5**, and **8** can be considered as dual materials as they combine SMM behavior and luminescent properties.

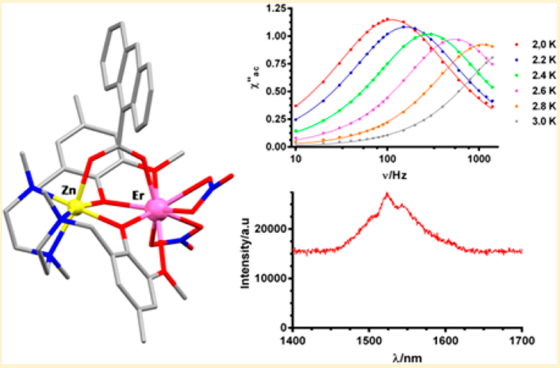

INTRODUCTION

Lanthanide coordination compounds have been the subject of intense research activity, especially due to their interesting magnetic and photophysical properties.[1,2] Their magnetic properties arise from the unpaired electrons in the inner f orbitals, which are very efficiently shielded by the fully occupied 5s and 5p orbitals and therefore interact very poorly with the ligand electrons. Because the ligand effects are very weak, most Ln^{III} complexes exhibit large and unquenched orbital angular momentum and consequently large intrinsic magnetic anisotropy and large magnetic moments in the ground state. Bearing this in mind, researchers have focused their attention toward lanthanide (and actinide) containing complexes, which could eventually behave as single-molecule magnets (SMMs)[3] or low temperature molecular magnetic coolers (MMCs).[4] SMMs show slow relaxation of the magnetization and magnetic hysteresis below the so-called blocking temperature (T_B), and have been proposed as potential nanomagnets for applications in molecular spintronics,[5] ultrahigh density magnetic information storage,[6] and quantum computing at molecular level.[7] The driving force behind the enormous increase of activity in the field of SMMs is the prospect of integrating them in nanosized devices.[8] MMCs show an enhanced magnetocaloric effect (MCE), which is based on the change of magnetic entropy upon application of a magnetic field and can potentially be used for cooling applications via adiabatic demagnetization. Both SMMs and MMCs require a large-spin multiplicity of the ground state (S_T), because in the former the energy barrier (Δ) that avoids the reversal of the molecular magnetization depends

Received: October 14, 2013
Published: December 17, 2013

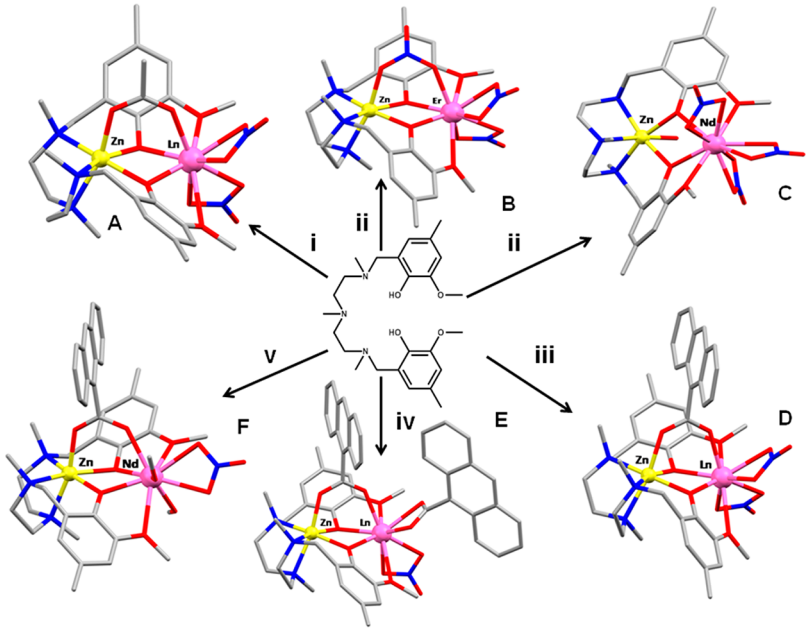

Figure 1. Structure of the ligand H_2L (center). (i) $H_2L/Zn(OAc)_2{\cdot}2H_2O/Ln(NO_3)_3{\cdot}nH_2O$, 1:1:1, in MeOH ($Ln^{III}$ = Tb (**1**), Dy (**2**), Er (**3**), Yb (**4**)). (ii) $H_2L/Zn(NO_3)_2{\cdot}6H_2O/Ln(NO_3)_3{\cdot}nH_2O$, 1:1:1, in MeOH ($Ln^{III}$ = Er (**5**), Nd (**6**)). (iii) $H_2L/Zn(NO_3)_2{\cdot}6H_2O/Ln(NO_3)_3{\cdot}nH_2O$/9-An/$Et_3N$. 1:1:1:1:1, in CH_3CN (Ln^{III} = Tb (**7**), Dy (**8**), Er (**9**), Yb (**10**)). (iii) Using the same conditions as in part i and recrystallization in CH_3CN (Yb (**11**)). The same conditions as in part iii (Nd (**12**)). (v) $H_2L/Zn(ClO_4)_2{\cdot}6H_2O/Nd(NO_3)_3{\cdot}6H_2O$//9-An/$Et_3N$, 1:1: 1:1:1, in MeOH (**13**).

on S^2, whereas in the latter the magnetic entropy is related to the spin by the expression $Sm = R\ \ln(2S + 1)$. However, the local anisotropy of the heavy Ln^{III} ions plays opposing roles in SMMs and MMCs. While highly anisotropic Ln^{III} ions (especially Dy^{III}) favor SMM behavior, MMCs require isotropic magnetic ions with weak exchange interactions generating multiple low-lying excited and field-accessible states, each of which can contribute to the magnetic entropy of the system, thus favoring the existence of a large MCE. Therefore, polynuclear (and high magnetic density) complexes containing the isotropic Gd^{III} ion with weak ferromagnetic interactions between the metal ions have been shown to be appropriate candidates for MMCs.[9]

As for photophysical properties, lanthanides exhibit intense, narrow-line, and long-lived (nanosecond, microsecond, or millisecond) emissions, which cover a spectral range from the near UV to the NIR region. Because f−f transitions are parity forbidden, the absorption coefficients are normally very low. However, organic ligands with strongly absorbing chromophores that transfer energy to the lanthanide can be used to circumvent that drawback (antenna effect).[10] For an efficient energy transfer the excited state of the ligand should be higher in energy than the lowest excited state of the lanthanide. It should be noted that lanthanide complexes have been applied as luminescent bioprobes in analyte sensing and tissues and cell imaging, as well as monitoring drug delivery. In particular, NIR luminescent complexes are of high interest due to their electronic and optical applications, especially for optical communications, and biological and sensor applications.[11]

Recently, we have designed a new compartmental ligand (H_2L: *N*,*N*′,*N*″-trimethyl-*N*,*N*″-bis(2-hydroxy-3-methoxy-5-methylbenzyl)diethylene triamine, see Figure 1) that presents two different coordination sites: an inner site of the N_3O_2 type showing preference for transition metal ions and the outer site (O_4) showing preference for hard, oxophilic metal ions such as lanthanides.[12a] The N_3O_2 pentacoordinated inner site forces metal ions with high preference for octahedral coordination to saturate their coordination sphere with a donor atom, which can proceed from a bridging ligand connecting the Ln and the transition metal ions. Following this strategy, a series of M^{II}−Ln^{III} (M^{II} = Mn, Ni, and Co) complexes were prepared with syn−syn carboxylate or nitrate bridging groups connecting M^{II} and Ln^{III} ions.[12] Moreover, the ligand does not contain active hydrogen atoms that would promote intermolecular hydrogen bonds thus allowing the formation of well isolated molecules in crystal lattice, favoring SMM behavior. The phenolic groups in this ligand assure the existence of ligand-centered electronic transitions in the near-UV, which could sensitize and enhance the emissive properties of Ln^{III} ions.

We,[12] and others,[13] have experimentally shown that the very weak $J_{M\text{-}Ln}$ observed for 3d/4f dinuclear complexes (M^{II} = Mn, Co, Ni, and Cu) leads to small effective energy barriers for the magnetization reversal. This can be due either to the small separations of the low lying split sublevels generated by the weak magnetic exchange interactions between the 3d and 4f metal ions or to the random transversal field for the Ln^{III} ions created by the paramagnetic metal ion, which favors the faster QTM process.[13b] In view of this, a good strategy to enhance the SMM properties of the 3d/4f aggregates would be that of eliminating the weak M^{II}−Ln^{III} interactions by replacing the paramagnetic M^{II} ions by a diamagnetic ion.[12e,13,14] According to this strategy, we are now pursuing, in a first step, the synthesis of 3d/4f systems with the H_2L ligand, in which the paramagnetic M^{II} ions have been replaced with diamagnetic Zn^{II}. Moreover, the new Zn^{II}−Ln^{III} complexes, in a similar manner to their analogous Schiff-base counterparts,[15] should exhibit interesting luminescent properties. Therefore, some of these complexes can behave as bifunctional materials, combining SMM and luminescent properties. In a second step, we are trying to improve the efficiency of energy transfer to the excited levels of the lanthanide ions in these complexes

dx.doi.org/10.1021/ic402597s | *Inorg. Chem.* 2014, 53, 1465−1474

by introducing a good antenna group, such as 9-anthracene carboxylate (9-An), connecting Zn^{II} and Ln^{III} ions.

Herein, we report the synthesis and X-ray structures of a series of $Zn^{II}Ln^{III}$ dinuclear complexes of formula $[Zn(\mu\text{-L})(\mu\text{-X})Ln(NO_3)_2]$ (X = none, NO_3^-, OAc^-, and 9-An; Ln^{III} = Dy, Tb, Er, Nd, Yb). Alternating current magnetic susceptibility studies reveal some slow relaxation of the magnetization. A study of their solid state photophysical properties has also been undertaken, especially of those complexes exhibiting emission in the NIR region (Ln^{III} = Er, Nd, Yb), with an enhanced NIR luminescence for the complexes containing 9-An bridging ligands discussed.

EXPERIMENTAL SECTION

General Procedures. Unless stated otherwise, all reactions were conducted in oven-dried glassware in aerobic conditions, with the reagents purchased commercially and used without further purification. The ligand H_2L was prepared as previously described.[12a]

Preparation of Complexes. *[Zn(μ-L)(μ-OAc)Ln(NO$_3$)$_2$] (Ln^{III} = Tb (**1**), Dy (**2**), Er (**3**), Yb (**4**)).* A general procedure was used for the preparation of these complexes: To a solution of H_2L (56 mg, 0.125 mmol) in 5 mL of MeOH were subsequently added with continuous stirring 27 mg (0.125 mmol) of $Zn(OAc)_2{\cdot}2H_2O$ and 0.125 mmol of $Ln(NO_3)_3{\cdot}nH_2O$. The resulting colorless solution was filtered and allowed to stand at room temperature. After two days, well formed prismatic colorless crystals of compounds **1** and **2**, pink crystals for **3**, and yellow crystals for **4** were obtained with yields in the range 40−55%, based on Zn.

*[Zn(μ-L)(μ-NO$_3$)Er(NO$_3$)$_2$] (**5**) and [Zn(H$_2$O)(μ-L)Nd(NO$_3$)$_3$]·2CH$_3$OH (**6**).* These compounds were prepared in a 60% yield as pink and violet crystals, respectively, following the procedure for **1**−**4**, except that $Zn(NO_3)_2{\cdot}6H_2O$ (37 mg, 0.125 mmol) was used instead of $Zn(OAc)_2{\cdot}2H_2O$.

*[Zn(μ-L)(μ-9-An)Ln(NO$_3$)$_2$]·2CH$_3$CN (Ln^{III} = Tb (**7**), Dy (**8**), Er (**9**), Yb (**10**); 9-An = 9-Anthracenecarboxylate).* To a solution of H_2L (56 mg, 0.125 mmol) in 5 mL of CH_3CN were subsequently added with continuous stirring 37 mg (0.125 mmol) of $Zn(NO_3)_2{\cdot}6H_2O$ and (0.125 mmol) of $Ln(NO_3)_3{\cdot}nH_2O$. To this solution was added dropwise another solution containing 28 mg of 9-anthracene-carboxylic acid (0.125 mmol) and 0.125 mmol of triethylamine. The resulting solution was filtered and the filtrate allowed to stand at room temperature for two days, whereupon colorless crystals of compounds **7** and **8**, pink for **9**, and yellow for **10** were obtained with yields in the range 40−50% based on Zn.

*[Zn(μ-L)(μ-9-An)Yb(9-An)(NO$_3$)$_2$]·3CH$_3$CN (**11**).* To a solution of H_2L (56 mg, 0.125 mmol) in 5 mL of MeOH were subsequently added with continuous stirring 37 mg (0.125 mmol) of $Zn(NO_3)_2{\cdot}6H_2O$ and 56 mg (0.125 mmol) of $Yb(NO_3)_3{\cdot}5H_2O$. To this solution was added dropwise another methanolic solution containing 28 mg of 9-anthracene-carboxylic acid (0.125 mmol) and 0.125 mmol of triethylamine, and immediately a yellow precipitate was obtained. The precipitate was dissolved in acetonitrile and the resulting solution filtered to eliminate any insoluble material. The filtrate was kept at room temperature for a week affording yellow crystals of compound **11** in 32% yield based on Zn.

*[Zn(μ-L)(μ-9-An)Nd(9-An)(NO$_3$)$_2$]·2CH$_3$CN·3H$_2$O (**12**).* To a solution of H_2L (56 mg, 0.125 mmol) in 5 mL of CH_3CN were subsequently added with continuous stirring 37 mg (0.125 mmol) of $Zn(NO_3)_2{\cdot}6H_2O$ and 55 mg (0.125 mmol) of $Nd(NO_3)_3{\cdot}6H_2O$. To this solution was added dropwise another solution containing 28 mg of 9-anthracene-carboxylic acid (0.125 mmol) and 0.125 mmol of triethylamine. The resulting solution was filtered and allowed to stand at room temperature for two days, whereupon violet crystals of **12** were obtained with a yield of 41% based on Zn.

*[Zn(μ-L)(μ-9-An)Nd(CH$_3$OH)$_2$(NO$_3$)](ClO$_4$)·2CH$_3$OH (**13**).* To a solution of H_2L (56 mg, 0.125 mmol) in 5 mL of MeOH were subsequently added with continuous stirring 46 mg (0.125 mmol) of $Zn(ClO_4)_2{\cdot}6H_2O$ and 56 mg (0.125 mmol) of $Nd(NO_3)_3{\cdot}5H_2O$. To this solution was added dropwise another methanolic solution containing 28 mg of 9-anthracene-carboxylic acid (0.125 mmol) and 0.125 mmol of triethylamine. The resulting solution was filtered and allowed to stand at room temperature. After one week, well-formed prismatic violet crystals of **13** were obtained with a yield of 38% based on Zn.

The purity of the complexes was checked by elemental analysis (see Supporting Information Table S1).

Physical Measurements. Elemental analyses were carried out at the "Centro de Instrumentación Científica" (University of Granada) on a Fisons-Carlo Erba analyzer model EA 1108. IR spectra on powdered samples were recorded with a ThermoNicolet IR200FTIR using KBr pellets. Alternating current susceptibility measurements under different applied static fields were performed using an oscillating ac field of 3.5 Oe and ac frequencies ranging from 1 to 1500 Hz with a Quantum Design SQUID MPMS XL-5 device. UV−vis spectra were measured on a UV-1800 Shimadzu spectrophotometer and the photoluminescence spectra on a Varian Cary Eclipse spectrofluorometer. Lifetime data were obtained on a JobinYvon-Horiba Fluorolog spectrometer fitted with a JY TBX picoseconds photodetection module. All near-IR photophysical data were obtained on a JobinYvon-Horiba Flourolog-3 spectrometer fitted with a Hamamatsu R5509-73 detector (cooled to −89 °C using a C9940 housing). For the near-IR lifetimes the pulsed laser source was a Continuum Minilite Nd:YAG configured for 355 nm output. Luminescence lifetime profiles were obtained using the JobinYvon-Horiba FluoroHub single photon counting module, and the data fits yielded the lifetime values using the provided DAS6 deconvolution software.

Single-Crystal Structure Determination. Suitable crystals of **1** and **3**−**13** were mounted on a glass fiber and used for data collection. Data for **1** were collected at 100(2) K on an Agilent Technologies SuperNova diffractometer (mirror-monochromated Mo Kα radiation, λ = 0.710 73 Å, Eos CCD detector) equipped with an Oxford Cryostream 700 PLUS temperature device. In all cases, data frames were processed (unit cell determination, intensity data integration, correction for Lorentz and polarization effects, and analytical absorption correction) using the CrysAlis software package.[16] Data for compounds **3**−**13** were collected with a Bruker AXS APEX CCD area detector equipped with graphite monochromated Mo Kα radiation (λ = 0.710 73 Å) by applying the ω-scan method. Lorentz-polarization and empirical absorption corrections were applied. The structures were solved by direct methods and refined with full-matrix least-squares calculations on F^2 using the program SHELXS97.[17] Anisotropic temperature factors were assigned to all atoms except for the hydrogens, which are riding their parent atoms with an isotropic temperature factor arbitrarily chosen as 1.2 times that of the respective parent. In the case of compound **12**, the hydrogen atoms associated with the water molecules O1W and O2W could not be directly located from difference Fourier maps. The highly disordered perchlorate anion in **13** could not be modeled, so that a new set of *F*2 (*hkl*) values with the contribution from the ClO_4^- anion withdrawn was obtained by the *SQUEEZE* procedure implemented in *PLATON*_94.[18]

Final $R(F)$, $wR(F^2)$, goodness of fit agreement factors, and details on the data collection and analysis can be found in Supporting Information Table S2. Selected bond lengths and angles are given in Supporting Information Table S3.

RESULTS AND DISCUSSION

As expected, the reaction of H_2L with $Zn(OAc)_2{\cdot}2H_2O$ and subsequently with $Ln(NO_3)_3{\cdot}nH_2O$ in MeOH and in 1:1:1 molar ratio led to crystals of the compounds $[Zn(\mu\text{-L})(\mu\text{-OAc})Ln(NO_3)_2]$ (Ln^{III} = Tb (**1**), Dy (**2**), Er (**3**), Yb (**4**)). The same reaction but using $Zn(NO_3)_3{\cdot}6H_2O$ instead of $Zn(OAc)_2{\cdot}2H_2O$ and $Ln(NO_3)_3{\cdot}6H_2O$ (Ln^{III} = Nd, Er) led to two different Zn−Ln dinuclear complexes $[Zn(\mu\text{-L})(\mu\text{-NO}_3)Er(NO_3)_2]{\cdot}2CH_3OH$ (**5**) and $[Zn(H_2O)(\mu\text{-L})Nd(NO_3)_3]{\cdot}2CH_3OH$ (**6**). Zn−Ln complexes, bearing a 9-anthracene carboxylate instead of acetate, connecting Zn^{II} and Ln^{III} ions of

dx.doi.org/10.1021/ic402597s | Inorg. Chem. 2014, 53, 1465−1474

formula $[Zn(\mu\text{-L})(\mu\text{-9-An})Ln(NO_3)_2]\cdot 2CH_3CN$ (Ln^{III} = Tb (**7**), Dy (**8**), Er (**9**), Yb (**10**)) could be prepared by reacting an acetonitrile solution containing H_2L, $Zn(NO_3)_3\cdot 6H_2O$, and $Ln(NO_3)_3\cdot nH_2O$ in 1:1:1 molar ratio with another acetonitrile solution containing 9-anthracene carboxylic acid and Et_3N in 1:1 molar ratio. Using the same reaction conditions as for complexes **1**−**4**, Yb^{III} leads to a yellow powder, which after recrystallization in acetonitrile afforded the compound of formula $[Zn(\mu\text{-L})(\mu\text{-9-An})Yb(9\text{-An})(NO_3)_2]\cdot 3CH_3CN$ (**11**) having both bridging and chelating bidentate 9-anthracenecarboxylate ligands, the latter coordinated to the Yb^{III} ion. With Nd^{III}, and using the same reaction conditions as for complexes **7**−**10**, only violet crystals of the compound $[Zn(\mu\text{-L})(\mu\text{-9-An})Nd(9\text{-An})(NO_3)_2]\cdot 2CH_3CN\cdot 3H_2O$ (**12**), whose structure is very similar to **11**, were obtained. However, with methanol as solvent and $Zn(ClO_4)\cdot 6H_2O$ instead of $Zn(NO_3)_2\cdot 6H_2O$, violet crystals of the complex $[Zn(\mu\text{-L})(\mu\text{-9-An})Nd(CH_3OH)_2(NO_3)](ClO_4)\cdot 2CH_3OH$ (**13**) were obtained (see Figure 1).

Crystal Structures. A perspective view of the structures of complexes **1**−**13** are given in Figure 1, whereas selected bond lengths and angles are given in Supporting Information Table S3.

Complex **1** is isostructural to those previously reported by us for the Ni−Ln and Co−Ln analogues and crystallizes in the triclinic $P\bar{1}$ space group.[12a−c] The structure of **1** consists of two almost identical dinuclear Zn^{II}−Tb^{III} molecules, in which the Tb^{III} and Zn^{II} ions are bridged by two phenoxo groups of the L^{2-} ligand and one *syn*−*syn* acetate anion. Compounds **3** and **4** crystallize in the monoclinic $P2_1/n$ space group, and its structure is very similar to that of **1** but having only one crystallographically independent Zn^{II}−Ln^{III} molecule. The structure of **2** was previously reported by us and is isostructural to that of **1**.[12a]

The structures of complexes **1**−**4** are given in Figure 1A. In all these complexes, the Zn^{II} ion exhibits a slightly trigonally distorted octahedral ZnN_3O_3 coordination polyhedron, where the three nitrogen atoms from the amine groups, and consequently the three oxygen atoms, belonging to the acetate and phenoxo bridging groups, occupy *fac* positions. The Zn−O and Zn−N distances are found in the ranges 2.037(3)−2.189(2) Å and 2.164(2)−2.262(2) Å, respectively. In all complexes, the corresponding Ln^{III} ion exhibits a LnO_9 coordination sphere, consisting of the two phenoxo bridging oxygen atoms, the two methoxy oxygen atoms, one oxygen atom from the acetate bridging group, and four oxygen atoms belonging to two bidentate nitrate anions. The LnO_9 coordination sphere is rather asymmetric, exhibiting short $Ln-O_{phenoxo}$ and $Ln-O_{acetate}$ bond distances in the range 2.2−2.3 Å and longer $Ln-O_{nitrate}$ and $Ln-O_{methoxy}$ bond distances >2.4 Å (one of the methoxy groups is weakly coordinated with Ln−O bond distances >2.6 Å). As expected, the average $Ln-O_{phenoxo}$ bond distances for compounds **1**−**4** steadily decrease from Tb^{III} to Er^{III} following the lanthanide contraction, with a concomitant decrease of the average Zn−Ln and $Ln-O_{acetate}$ bond distances.

The Zn(di-μ-phenoxo)(μ-acetate)Ln bridging fragment is rather asymmetric, not only because the $Ln-O_{phenoxo}$ and $Zn-O_{phenoxo}$ bond distances are different, but also because there exists two different Zn−O−Ln bridging angles with average values of 106.28° and 100.5° for complexes **1**−**4**.

The bridging acetate group forces the structure to be folded with the average hinge angle of the M(μ-O_2)Ln bridging fragment ranging from 23.39° for **1** to 22.55° for **3** (the hinge angle, β, is the dihedral angle between the O−Zn−O and O−Ln−O planes in the bridging fragment). Therefore, the hinge angle increases with the decrease of the Ln^{III} size, as expected.

The structure of $[Zn(\mu\text{-L})(\mu\text{-}NO_3)Er(NO_3)_2]\cdot 2CH_3OH$ (**5**) is isostructural with two Ni−Ln complexes,[12a,b] previously reported by us and very similar to that of compounds **1**−**4** but having a bridging nitrate anion connecting the Er^{III} and Zn^{II} metal ions instead of an acetate anion (see Figure 1B). Compared to complex **3**, the most significant effect of the coordination of the nitrato bridging ligand in **5** is that the Zn(μ-O_2)Er bridging fragment is folded to a lesser extent. Thus, the hinge angle decreases from 22.6° in **3** to a 14.4° in **5**, with a simultaneous decrease of Er−O−Zn angles at the bridging region, as well as the out-of-plane displacements of the O−C bonds belonging to the phenoxo bridging groups from the $Zn(O)_2Er$ plane. At variance with **3**, where the acetate and metal ions are almost coplanar, in **5** the plane of the nitrate anion and the plane containing the Zn^{II}, Er^{III}, and the two oxygen atoms of the nitrato bridging ligands coordinated to the metal ions, form a dihedral angle of 28.6°. Zn−O and Er−O bond distances, involving the oxygen atoms of the nitrate anion in **5**, are more than 0.1 Å longer than those involving the acetate bridging group in **3**. The rest of the distances and angles in **5** are very close to that found in **3** and do not deserve any further discussion.

Compound **6** was prepared using the same reaction conditions as for **5**, but it does not contain a nitrate anion connecting the Nd^{III} and Zn^{II} ions. This may be due to the fact that the large Nd^{III} ion could enforce a significant strain in the weakly bonded nitrate bridging ligand, so that the di-μ-phenoxo-bridged would be more favorable than the diphenoxo-nitrate-bridged one. The structure of **6** is given in Figure 1C and consists of $[Zn(H_2O)(\mu\text{-L})Nd(NO_3)_3]$ neutral molecules and two methanol molecules of crystallization, both of which are involved in hydrogen bond interactions. As expected, the absence of a nitrate bridging group in **6** gives rise to a more planar Zn(μ-O_2)Nd bridging fragment with a hinge angle of 6.6°. Moreover, a water molecule saturates the octahedral coordination sphere of the Zn^{II} ion, and most importantly, the coordination of one additional bidentate chelating nitrate ligand to the Nd^{III} ion leads to an expanded and more symmetrical NdO_{10} coordination sphere.

Finally, it should be stressed that **6** exhibits both intermolecular and intramolecular hydrogen bond interactions. The former involve the molecules of methanol, the coordinated water molecule, and one of the nitrate anions belonging to two centrosymmetrically related Zn^{II}−Nd^{III} molecules with donor−acceptor distances in the range 2.623−2.823 Å. The latter involve the water molecule and one of the nitrate anions of the same Zn^{II}−Nd^{III} moiety with O···O distances of 2.920 Å.

The structures of complexes **7**−**10** are shown in Figure 1D and are very similar to those of complexes **1**−**4** but with a 9-anthracenecarboxylate bridging ligand instead of an acetate ligand connecting the Zn^{II} and Ln^{III} ions, and with two acetonitrile molecules of crystallization. Compared to **1**−**4**, the acetate bridged analogues, compounds **7**−**10**, exhibit a small hinge angle and smaller and closer Zn−O−Dy bridging angles, resulting in a smaller degree of asymmetry in the bridging region. One of the $Dy-O_{methoxy}$ bond distances is significantly shorter than those in complexes **1**−**4**, leading to less asymmetry in the DyO_9 coordination sphere. The plane of the anthracene ring is not coplanar with the corresponding plane of carboxylate

dx.doi.org/10.1021/ic402597s | Inorg. Chem. 2014, 53, 1465−1474

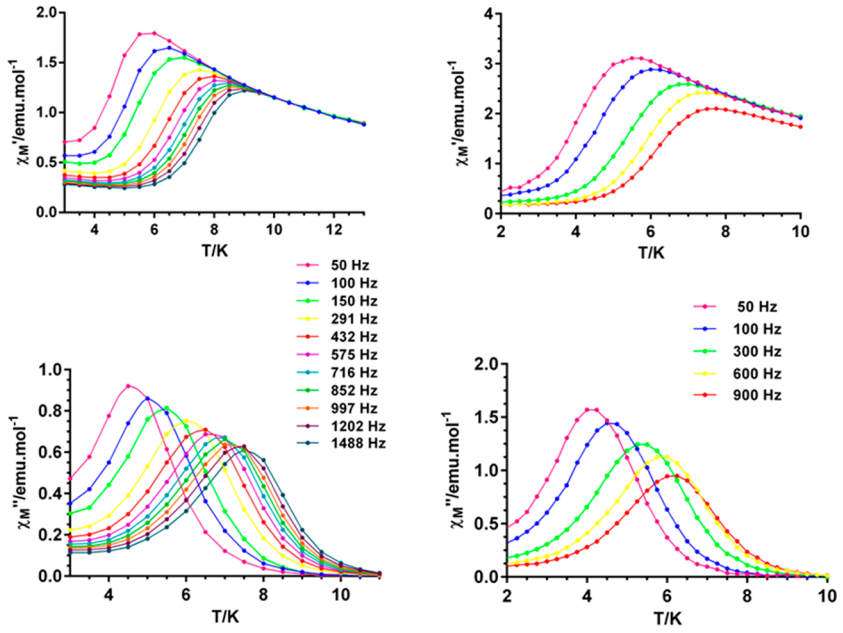

Figure 2. Temperature dependence of in-phase χ'_M (top) and out-of-phase χ''_M (bottom) components of the ac susceptibility for complexes **2** (left) and **8** (right) measured under 1000 Oe applied dc field.

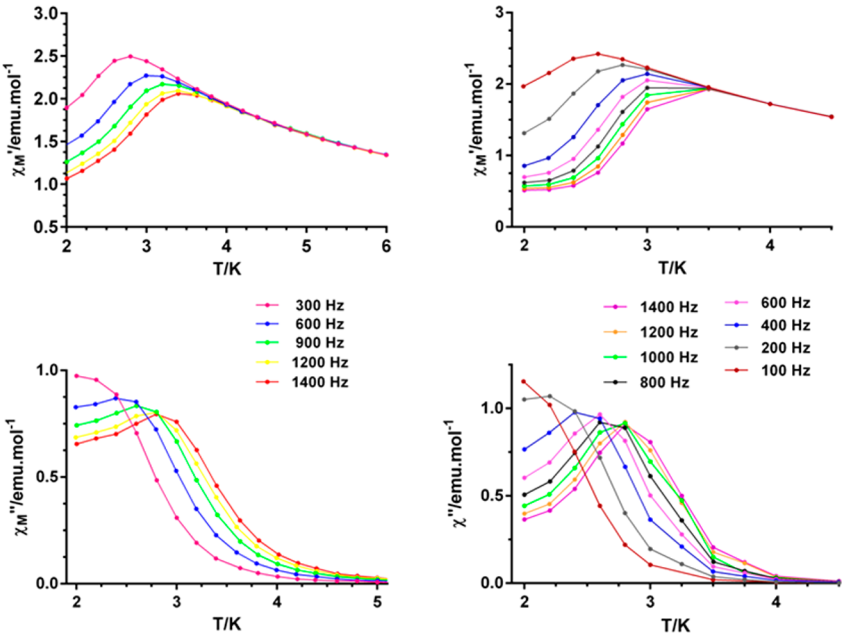

Figure 3. Temperature dependence of in-phase χ'_M (top) and out-of-phase χ''_M (bottom) components of the ac susceptibility for complexes **3** (left) and **5** (right) measured under 1000 Oe applied dc field.

group, having a dihedral angle between these planes of ∼84°. Bond distances and angles in the rest of the molecule are very close to those observed in the acetate bridged counterparts.

Compounds **11** and **12** have very similar structures, containing two 9-anthracene carboxylate bidentate ligands: one acting as a bridge linking the Zn^{II} and Ln^{III} ions and the other one acting as a chelating ligand coordinated to the Ln^{III} ion (Figure 1E). As with the Ni^{II}–Dy^{III} analogue,[12b] these compounds crystallize in a noncentrosymmetric space group (orthorhombic, $Pca2_1$) and therefore are examples of chiral molecules obtained from achiral starting materials. The overall ensemble of crystals in a batch of **11** and **12** is expected to contain crystals of both enantiomeric forms in equal amounts and therefore to be racemic. As in compounds **7**–**10**, the anthracene rings are not coplanar with the corresponding plane of carboxylate group, with dihedral angles between these planes of ∼89° and ∼82°, for the bridging and chelating 9-anthracene carboxylate ligands (9-An), respectively, whereas the dihedral angle between the planes of the anthracene rings for the two 9-An ligands is ∼55°. The Ln–O bond distances involving the oxygen atoms of the chelating 9-anthracene carboxylato are shorter than the $Ln–O_{nitrate}$ ones (∼0.1 Å), the $Ln–O_{methoxy}$ are the longest and rather different (∼ 0.2 Å), and the two $Ln–O_{phenoxo}$ distances are ∼0.1 Å shorter than the $Ln–O_{carboxylate}$, so that the LnO_9 coordination sphere is rather asymmetric.

dx.doi.org/10.1021/ic402597s | Inorg. Chem. 2014, 53, 1465–1474

The structure of **13** is similar to those of compounds **7**−**10**, but one of the nitrate bidentate ligands coordinated to the Ln^{III} ion is replaced by two molecules of methanol that adopt a *cis* configuration. The structure of **13** (see Figure 1F) consists of positive dinuclear units $[Zn(\mu\text{-L})(\mu\text{-9-An})Nd(CH_3OH)_2(NO_3)]^+$, a perchlorate anion, and two methanol molecules of crystallization. Nd−O distances are in the range 2.30−2.69 Å, and therefore the LnO_9 coordination sphere is the least asymmetric in this series of Zn^{II}−Ln^{III} complexes. Centrosymmetrically related molecules are held in pairs by four complementary hydrogen bonds involving one of the methanol molecules of crystallization, which forms two bifurcated hydrogen bonds with the noncoordinated oxygen atom of the bidentate nitrate anion and one of the coordinated methanol molecules of a neighboring unit with O···O distances of 2.977 and 2.651 Å, respectively.

SMM Behavior. In order to know if our strategy of replacing the 3d paramagnetic ion by Zn^{II} in diphenoxo-bridged 3d−4f systems improves the SMM properties of this kind of compound, we have performed dynamic ac magnetic susceptibility measurements as a function of both temperature and frequency. Under zero-external field, only compound **8** exhibits a weak frequency dependence of the out-of-phase signal, χ''_M, below 10 K without a net maximum above 2 K, even at frequencies as high as 1400 Hz (see Supporting Information Figure S1). This behavior indicates that either the energy barrier for the flipping of the magnetization is not high enough to trap the magnetization in one of the equivalent configurations above 2 K or there exists quantum tunneling of the magnetization (QTM), leading to a flipping rate that is too fast to observe the maximum in the χ''_M above 2 K. The fact that χ''_M for **8** below 4 K does not go to zero but increases very sharply is a clear indication of the existence of QTM. This fast relaxation process can be promoted by transverse anisotropy, and dipolar and hyperfine interactions. Nevertheless, for Kramers ions such as Dy^{III}, the first mechanism would not facilitate the QTM relaxation process. When the ac measurements were performed in the presence of a small external dc field of 1000 G to fully or partly suppress the quantum tunneling relaxation of the magnetization, the Dy compounds **2** and **8** and the Er compounds **3** and **5** showed typical SMM behavior with maxima in the 6.75 K (1488 Hz)−4.25 K (50 Hz), 6.5 K (900 Hz)−4.25 K (50 Hz), 3 K (1400 Hz)−2.5 K (600 Hz), and 2.75 K (1400 Hz)−2.2 K (400 Hz) ranges, respectively (Figures 2 and 3).

The relaxation times, τ's, for compounds **2**, **8**, and **5** were extracted from the fit of the frequency dependence of χ_M'' at each temperature to the generalized Debye model (Supporting Information Figures S2−S3). In the case of compound **3**, that does not exhibit any maximum in the χ_M'' versus frequency plot (the same fit as for compounds **2**, **8**, and **5** does not lead to reliable values of τ), the temperatures and frequencies of the maxima in the χ_M'' versus T plot were used to extract the relaxation times. The results were then used in constructing the Arrhenius plot, $\tau = \tau_0 \exp(\Delta/k_BT)$, shown in Supporting Information Figures S2−S3. The fit of the high temperature linear portions of the data afforded the effective energy barriers for the reversal of the magnetization Δ and τ_o values indicated in Table 1. The Arrhenius plots, constructed from the temperatures and frequencies of the maxima observed for the χ''_M signals in Figures 2 and 3 for compounds **2**, **5**, and **8**, lead virtually to the same Δ and τ_0 (flipping rate) parameters, as expected. The fact that the out-of-phase susceptibility for these compounds tends to zero after the maxima is a clear indication that the QTM is suppressed. Only for compound **3** is the suppression of the QTM incomplete, which may be due to the existence of significant intermolecular interactions. In some cases, the effects of these interactions, that favor the fast QTM process, cannot be eliminated by application of a small magnetic dc field.

Table 1. Δ and τ_0 Values for Compounds 2, 3, 5, and 8

compd	χ''_M signal at H = 0 Oe	Δ(K) at H = 1000 Oe	τ_0 (s)
2	yes	41(2)	5.6×10^{-7}
3	no	11.7(3)	2.0×10^{-6}
5	no	22(2)	5.3×10^{-8}
8	no	32.1(3)	1.9×10^{-6}

[a]Direct current magnetic properties (including $\chi_M T$ vs T and M vs H plots) for these compounds are given in the Supporting Information as Figures S5 and S6).

The Cole−Cole diagrams for these complexes are shown in Supporting Information Figure S4. The Cole−Cole plots for complexes **2**, **5**, and **8** are rather symmetrical, and in the high temperature regions corresponding to the linear portion of the data in the Arrhenius plots, they exhibit semicircular shapes with α values in the ranges 0.02 (8 K)−0.10 (5 K), 0.1(3 K)−0.15 (2.2 K), 0.06 (6.75 K)−0.19 (5 K) for **2**, **5**, and **8**, respectively. These low α values indicate very narrow distribution of slow relaxation in these regions, which would be compatible with the existence of only one relaxation process. In the case of **3** the Cole−Cole diagram is nonsymmetrical with α values are in the range 0.06 (3 K)−0.29 (2.4 K), thus indicating that the crossover from the thermally activated relaxation process to a quantum regime occurs below ∼2.6 K.

The values of Δ/k_B found for **2** and **8** are near the center of the range experimentally observed for for mono- and polynuclear Dy SMMs.[1e] It should be noted that the maximum value of Δ found for M^{II}−Dy^{III} (M^{II} = Ni and Co) compounds isostructural to **2** and **8** was 19.2 K.[12a−c] Therefore, these results support the conclusion that replacement of the paramagnetic M^{II} metal ion by Zn^{II} can be an appropriate strategy to improve the SMM properties in diphenoxo-bridged 3d−4f systems. Complexes **2** and **8** exhibit very similar LnO_9 coordination spheres with a poorly defined geometry as they are intermediate between several nine-vertex polyhedra (see Supporting Information, Tables S4 and S5). Previous *ab initio* calculations on a Dy fragment of a Co−Dy compound isostructural to **2** clearly showed that the ground Kramers doublet arising from the ligand-field splitting of the $^6H_{15/2}$ ground atomic term shows strong axial anisotropy with g_z =18.9 (g_x = 0.06 and g_y = 0.09) along the main anisotropy axis, which lies close to the Dy−Co direction.[12c] The large axial anisotropy of the Dy^{III} ion in compounds **2** and **8** must therefore be at the origin of their SMM behavior. Notice that axial ligand fields induce strong easy axis anisotropy of Dy^{III} because it has an oblate electron density.[1a] This ligand field anisotropy is easy to achieve accidentally, and this is the reason why a wide variety of Dy^{III}-containing SMMs have been reported. In this regard, the ligand field created by the nine oxygen atom of the LnO_9 coordination sphere is not axial; however, **2** and **8** still present strong axial anisotropy and SMM behavior.

It should be noted that Er^{III} based SMMs are rare, and as far as we know, only three such examples have been reported. One of them, $Na_9[Er(W_5O_{18})_2]\cdot xH_2O$[19] (the Er^{III} ion is encapsulated between two diamagnetic polyoxometalate cages), exhibits

dx.doi.org/10.1021/ic402597s | Inorg. Chem. 2014, 53, 1465−1474

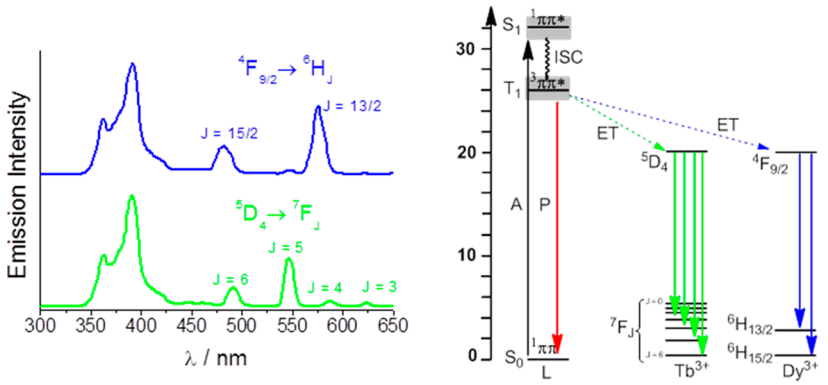

Figure 4. (a) Sensitized emission spectra of complexes **1** (green) and **2** (blue) in the solid state at room temperature. (b) Jablonski's diagram of complexes **1** and **2**; approximate energy values of the singlet (S_1) and triplet (T_1) states of the ligand H_2L were determined from its UV−vis absorption and emission spectra.

SMM behavior at zero field with a thermal energy barrier of 55.3 K. The other two are Zn_3Er complexes of very similar hexaimine planar macrocyclic ligands with six oxygen atoms bridging the Zn^{II} and Er^{III} ions.[20] The former displays a flattened D_{4d} antiprismatic LnO_8 coordination sphere leading to a $M_J = \pm 13/2$ ground state that is separated from the first excited state by ~30 cm^{-1}, whereas the other two have LnO_9[20a] and suspected LnO_{10}[20b] coordination spheres that conserve a strong equatorial ligand field. Er^{III} has prolate electron density,[1a] and to generate single-ion anisotropy and SMM behavior, an equatorial ligand field is, in principle, required. The two Zn_3Er^{III} complexes are examples of systems having this kind of ligand field, whereas the Er−POM system exhibits a ligand field that can be considered as intermediate between axial and equatorial. For complexes **3** and **5**, with LnO_9 coordination spheres very similar to that of **2** and **8** (see Supporting Information, Tables S6 and S7), the absence of a clear axial field can allow an easy-axis anisotropy leading to the observed SMM behavior.

It is worth mentioning that the field dependence of the magnetization for complexes **2**, **3**, **5**, and **8** shows no significant hysteresis above 2 K with the sweep rates used in the SQUID magnetometer (see Supporting Information Figure S7).

Photophysical Properties. In the past few years, several examples of lanthanide complexes coordinated by compartmental Salen-type Schiff-base ligands have been reported to exhibit interesting photophysical properties. These ligands act as antenna groups, sensitizing Ln^{III}-based luminescence through an intramolecular energy transfer process.[15] Considering the similarity between ligand H_2L and those Salen-derivates, the photophysical properties of samples **1**−**6** have been studied to determine the ability of ligand L^{2-} to act as sensitizer. The photophysical properties of complexes **7**−**13**, which additionally contain 9-anthracene carboxylate ligands in their structure, have also been analyzed. The reflectance spectrum of ligand H_2L (Supporting Information Figure S8) shows intense absorption bands in the UV region located at 240 and 290 nm, which are typical of intraligand $\pi-\pi^*$ electronic transitions in the aromatic groups. Excitation at 290 nm resulted in the appearance of a weak ligand-centered emission (Supporting Information Figure S8, inset) with a maximum located at λ_{em} = 391 nm and a shoulder located at higher energy (λ_{em} = 365 nm).

The 9-anthracene carboxylate ligand is a well-known luminophore, and anthracene derivates have been previously used as antenna groups to sensitize Ln^{III}-based luminescence in the NIR region.[21] This ligand shows characteristic $\pi-\pi^*$ absorption bands that extend well into the visible region and display an intense and broad emission band centered at *ca.* 500 nm.

In all cases, we examined the emissive properties of the complexes as microcrystalline powders, with their poor solubility preventing detailed study of their photophysical properties in solution.

First, we examined the emissive properties of complexes **1** and **2** where the respective Tb^{III} and Dy^{III} ions are potential emitters in the visible region which can be sensitized by an energy transfer from the L^{2-} ligand. In both cases, excitation into the UV $\pi-\pi^*$ absorption band of ligand L^{2-} at 290 nm resulted in the appearance of the characteristic Tb^{III} ($^5D_4\rightarrow {}^7F_J$; J = 3, 4, 5, 6) and Dy^{III} ($^4F_{9/2}\rightarrow {}^6H_{J/2}$; J = 15/2, 13/2) emission bands in the visible region, respectively (Figure 4). This sensitized Ln^{III}-based emission can only occur through a L → Ln photoinduced energy transfer process, which probes the ability of ligand L^{2-} to act as an antenna group. However, a significant residual ligand-centered emission is still observed which indicates that the energy transfer process is not complete. The same behavior has been recently observed for some mononuclear Dy^{III} complexes containing the 9-diethylphosphonomethyl anthracene ligand.[22]

Similarly, the photophysical properties of samples **7** and **8** were studied. Both complexes contain the bridging ligand 9-anthracene carboxylate directly linked to the lanthanide ions. In these cases, excitation of the complexes into the UV absorption manifold of the 9-anthracene carboxylate unit ($\lambda_{ex.}$ = 355 nm) did not result in sensitized Ln^{III} emission in the visible region. In both cases, only the characteristic emission of the anthracene moiety was observed. This is due to the fact that the energy of the emissive $^3\pi\pi^*$ state is lower than that of the emissive $^5D_4$ and $^4F_{9/2}$ excited states of ions Tb^{III} and Dy^{III}, respectively.

Regarding the expected sensitized emission characteristic of ions Er^{III} ($^4I_{13/2}\rightarrow {}^4H_{15/2}$; λ_{em} = 1530 nm) in **3** and **5**, Yb^{III} ($^2F_{5/2}\rightarrow {}^2F_{7/2}$; λ_{em} = 980 nm) in **4** and Nd^{III} [$^4F_{3/2}\rightarrow {}^4F_J$; J = 11/2 (λ_{em} = 1060 nm), 13/2 (λ_{em} = 1340 nm)] in **6**, only the emission characteristic of Yb^{III} ions in **4** was observed (Supporting Information Figure S9) when the compound was excited at 290 nm, which indicates the low efficiency of ligand

dx.doi.org/10.1021/ic402597s | *Inorg. Chem.* 2014, 53, 1465−1474

L^{2-} to act as antenna group for these ions. This is probably due to the poor spectroscopic overlap existing between the ligand emission and the f−f excited states of ions Er^{III}, Nd^{III}, and Yb^{III} that could act as energy acceptors. Nevertheless, time-resolved luminescent experiments performed on these samples using a Nd:YAG excitation source with λ_{ex} = 355 nm allowed us to determine the emission lifetime characteristics of ions Er^{III}, Nd^{III}, and Yb^{III} in these samples. These lifetimes, obtained after fitting the luminescent decay curve monoexponentially, are collected in Table 2, and their values are within those commonly observed for Nd^{III}, Er^{III}, and Yb^{III} molecular complexes, typically 2 μs for Er^{III}, 1 μs for Nd^{III}, and 10 μs for Yb^{III}.[23]

Table 2. Luminescence Lifetimes of the Solid Samples 3−6 and 9−13[a]

complex	τ (μs)	complex	τ (μs)
3	2.08	**9**	2.77
4	10.3	**10**	6.86
5	0.47	**11**	11.82
6	2.14	**12**	0.80
		13	1.12

[a]Measured at room temperature using 355 nm excitation.

This demonstrates that ligand L^{2-} can sensitize Ln^{III}-based emission, although the efficiency of the energy transfer process is rather low. To improve the NIR Ln^{III}-based emissive properties of this kind of molecule, the organic ligand 9-anthracene carboxylate was introduced as a bridging ligand in complexes **9**−**13**. In addition, for samples **11** and **12**, a second anthracene unit is directly chelated to the lanthanide ion. As expected, in all these cases, excitation at 355 nm resulted in the appearance of intense sensitized NIR emission from ions Er^{III} (**9**), Nd^{III} (**12**, **13**), and Yb^{III} (**10**, **11**) at their characteristic wavelengths (Figure 5).

These results confirm that the use of 9-anthracene carboxylate ligands as bridging and/or chelate ligands directly coordinated to the Ln^{III} ions significantly improves their NIR luminescent properties.

CONCLUSIONS

We have demonstrated that the compartmental ligand H_2L (*N*,*N*′,*N*″-trimethyl-*N*,*N*″-bis(2-hydroxy-3-methoxy-5-methylbenzyl)-diethylenetriamine) allows the preparation of four series of dinuclear Zn^{II}−Ln^{III} complexes, in which the Zn^{II} ion occupies the internal N_3O_2 site and the oxopholic Ln^{III} ion occupies the external O_4 site, leading to diphenoxo-bridged species. The sixth position in the Zn^{II} coordination sphere is occupied by either a water molecule or the oxygen atom belonging to acetate, nitrate, or 9-anthracenecarboxylate bridging groups, leading to doubly bridged diphenoxo or triply bridged diphenoxo-acetate, diphenoxo-nitrate, and diphenoxo-antracene carboxylate complexes, respectively. Dynamic ac magnetic susceptibility measurements as a function of temperature and frequency show that the Dy^{III} complexes **2** and **8** and the Er^{III} derivates **3** and **5** exhibit field-induced SMM behavior with effective thermal energy barriers of 41, 32.1, 11.7, and 22 K, respectively. These are larger than those found for isostructural complexes with paramagnetic 3d ions such as Ni^{II}, and Co^{II}, suggesting that the replacement of paramagnetic ions by diamagnetic ions is one strategy for increasing U_{eff} in 3d/4f systems. The increase in U_{eff} appears to due to the elimination of the weak magnetic exchange coupling between 3d and 4f ions that either leads to a small energy separation between the ground and first excited state or allows the existence of a transversal field for the Ln^{III} ion created by the paramagnetic 3d metal ion. Moreover, we believe that, as observed in other systems containing diamagnetic ions, the existence of a diamagnetic Zn^{II} ion linked to the Ln^{III} ions mitigates the intermolecular interactions between the Ln^{III}, thus diminishing the QTM process and favoring the observation of slow relaxation of the magnetization. Complexes **3** and **5** are very rare examples of Er^{III}-containing SMMs.

Finally, the photophysical properties of these complexes have been studied, and the ability of the ligand L^{2-} to sensitize Tb^{III}- and Dy^{III}-based luminescence in the visible region has been demonstrated. For complexes **1** and **2**, excitation of the $\pi\pi^*$ absorption of the ligand results in concomitant sensitized emission in the visible region from the Tb^{III} and Dy^{III} units, respectively. However, the efficiency of this ligand to sensitize the characteristic emission from Er^{III}, Nd^{III}, and Yb^{III} ions in the

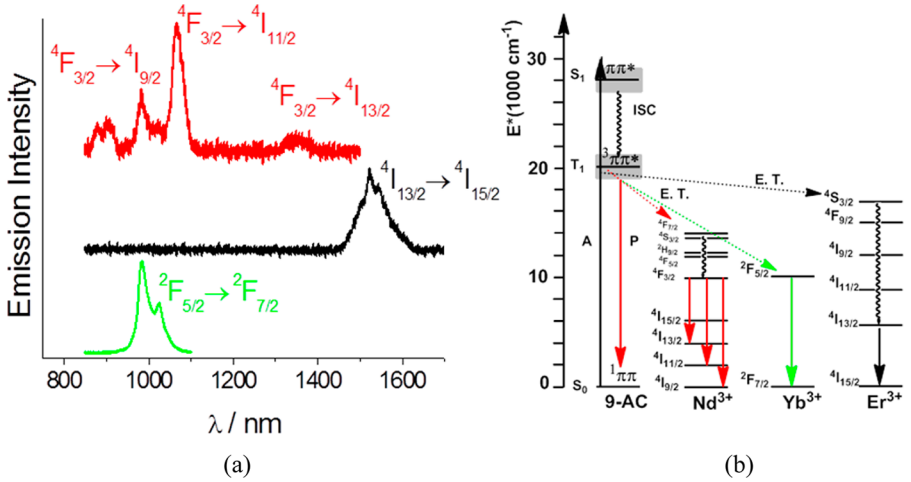

Figure 5. (a) NIR sensitized emission spectra of complexes **9** (black), **10** (green), and **12** (red) in solid state at room temperature. (b) Jablonski's diagram of these complexes; approximate energy values of the singlet and triplet states of the ligand 9-anthracene carboxylic acid (S_1 and T_1) were determined from its UV−vis absorption and emission spectra, respectively.

dx.doi.org/10.1021/ic402597s | Inorg. Chem. 2014, 53, 1465−1474

NIR region is rather low due to the poor spectroscopic overlap existing between the ligand emission and the f−f excited states of these ligands. Introducing a 9-anthracene carboxylate as a bridging and/or chelating ligands for the ions enhanced NIR emission in these systems.

Dy^{III} complexes **2** and **8** and Er^{III} complexes **3** and **5** combine field-induced SMM behavior and luminescent properties and therefore can be considered as examples of dual magnetic-luminescent materials.[24]

■ ASSOCIATED CONTENT

Supporting Information

Elemental analyses for all the complexes. X-ray crystallographic data, including data in CIF format, for **1**, **3**−**13**, including data collection, refinement, and selected bond lengths and angles. Variable-temperature frequency dependence of the ac out-of-phase χ_M'' signal for complexes **2**, **5**, and **8**. Cole−Cole plots for complexes complexes **2**, **3**, **5**, and **8**. Reflectance spectrum of the ligand and photoluminescence spectrum of compound **4**. This material is available free of charge via the Internet at http://pubs.acs.org.

■ AUTHOR INFORMATION

Corresponding Author

*E-mail: ecolacio@ugr.es.

Notes

The authors declare no competing financial interest.

■ ACKNOWLEDGMENTS

Financial support from the Spanish Ministerio de Ciencia e Innovación (MICINN) (Project CTQ-2011-24478), the Junta de Andalucía (FQM-195, the Project of excellence P11-FQM-7756), and the University of Granada is acknowledged. S.T.-P. thanks the Junta de Andalucía for a research grant. E.K.B. thanks the EPSRC for funding.

Technical and human support provided by SGIker (UPV/EHU, MINECO, GV/EJ, ERDF, and ESF) and CIC (University of Granada) are gratefully acknowledged.

■ REFERENCES

(1) (a) Rinehart, J. D.; Long, J. R. *Chem. Sci.* **2011**, *2*, 2078. (b) Sorace, L.; Benelli, C.; Gatteschi, D. *Chem. Soc. Rev.* **2012**, *42*, 3278. (c) Luzon, J.; Sessoli, R. *Dalton Trans.* **2012**, *41*, 13556. (d) Clemente-Juan, J. M.; Coronado, E.; Gaita-Ariño, A. *Chem. Soc. Rev.* **2012**, *41*, 7464. (e) Woodruff, D. N.; Winpenny, R. E. P.; Layfield, R. A. *Chem. Rev.* **2013**, *113*, 5110.

(2) (a) Ward, M. D. *Coord. Chem. Rev.* **2007**, *251*, 1663. (b) Binnemans, K. *Coord. Chem. Rev.* **2009**, *109*, 4283. (c) Bünzli, J. C. G. *Acc. Chem. Res.* **2006**, *39*, 53.

(3) Gatteschi, D.; Sessoli, R.; Villain, J. *Molecular Nanomagnets*; Oxford University Press: Oxford, U.K., 2006.

(4) Evangelisti, M.; Brechin, E. K. *Dalton Trans.* **2010**, *39*, 4672.

(5) Bogani, L.; Wernsdorfer, W. *Nat. Mater.* **2008**, *7*, 179.

(6) (a) Rocha, A. R.; García-Suárez, V. M.; Bailey, S. W.; Lambert, C. J.; Ferrerand, J.; Sanvito, S. *Nat. Mater.* **2005**, *4*, 335. (b) Affronte, M. *J. Mater. Chem.* **2009**, *19*, 1731.

(7) (a) Leuenberger, M. N.; Loss, D. *Nature* **2001**, *410*, 789. (b) Ardavan, A.; Rival, O.; Morton, J. J. L.; Blundell, S. J.; Tyryshkin, A. M.; Timco, G. A.; Winpenny, R. E. P. *Phys. Rev. Lett.* **2007**, *98*, 057201. (c) Stamp, P. C. E.; Gaita-Ariño, A. *J. Mater. Chem.* **2009**, *19*, 1718.

(8) (a) Candini, A.; Klyatskaya, S.; Ruben, M.; Wernsdorfer, W.; Affronte, M. *Nano Lett.* **2011**, *11*, 2634. (b) Vincent, R.; Klyatskaya, S.; Ruben, M.; Wernsdorfer, W.; Balestro, F. *Nature* **2012**, *488*, 357. (c) Ganzhorn, M.; Klyatskaya, S.; Ruben, M.; Wernsdorfer, W. *Nat. Nanotechnol.* **2013**, *8*, 165.

(9) (a) Evangelisti, M.; Roubeau, O.; Palacios, E.; Camón, A.; Hooper, T. N.; Brechin, E. K.; Alonso, J. J. *Angew. Chem., Int. Ed.* **2011**, *50*, 6606. (b) Lorusso, G.; Palacios, M. A.; Nichol, G. S.; Brechin, E. K.; Roubeau, O.; Evangelisti, M. *Chem. Commun.* **2012**, *48*, 7592.

(10) (a) Bünzli, J. C. G.; Piguet, C. *Chem. Soc. Rev.* **2005**, *34*, 1048. (b) Parker, D. *Chem. Soc. Rev.* **2004**, *33*, 156. (c) Hasegawa, Y.; Wada, Y.; Yanayida, S. *J. Photochem. Photobiol., C* **2004**, *5*, 183.

(11) (a) Bünzli, J. C. G. *Chem. Rev.* **2010**, *110*, 2729. (b) Faulkner, S.; Pope, S. J. A.; Burton-Pye, B. P. *Appl. Spectrosc. Rev.* **2005**, *40*, 1. (c) Lin, S. *Chem. Soc. Rev.* **2004**, *33*, 445.

(12) (a) Colacio, E.; Ruiz-Sanchez, J.; White, F. J.; Brechin, E. K. *Inorg Chem.* **2011**, *50*, 7268. (b) Colacio, E.; Ruiz, J.; Mota, A. J.; Palacios, M. A.; Cremades, E.; Ruiz, E.; White, F. J.; Brechin, E. K. *Inorg. Chem.* **2012**, *51*, 5857. (c) Colacio, E.; Ruiz, J.; Mota, A. J.; Palacios, M. A.; Ruiz, E.; Cremades, E.; Hänninen, M. M.; Sillanpää, R.; Brechin, E. K. *C. R. Chim.* **2012**, *15*, 878. (d) Colacio, E.; Ruiz, J.; Ruiz, E.; Cremades, E.; Krzystek, J.; Carretta, S.; Cano, J.; Guidi, T.; Wernsdorfer, W.; Brechin, E. K. *Angew. Chem., Int. Ed.* **2013**, *52*, 9130. (e) Titos-Padilla, S.; Ruiz, J.; Herrera, J. M.; Brechin, E. K.; Wersndorfer, W.; Lloret, F.; Colacio, E. *Inorg. Chem.* **2013**, *52*, 9620.

(13) (a) Watanabe, A.; Yamashita, A.; Nakano, M.; Yamamura, T.; Kajiwara, T. *Chem.—Eur. J.* **2011**, *17*, 7428. (b) Bhunia, A.; Gamer, M. T.; Ungur, L.; Chibotaru, L. F.; Powell, A. K.; Lan, Y.; Roesky, P. W.; Menges, F.; Riehn, C.; Niedner-Schatteburg, G. *Inorg. Chem.* **2012**, *51*, 9589.

(14) Yamashita, A.; Watanabe, A.; Akine, S.; Nabeshima, T.; Nakano, M.; Yamamura, T.; Kajiwara, T. *Angew. Chem., Int. Ed.* **2011**, *50*, 4016.

(15) (a) Bi, W. Y.; Lü, X. Q.; Chai, W. L.; Wei, T.; Song, J. R.; Zhao, S. S.; Wong, W. K. *Inorg. Chem. Commun.* **2009**, *12*, 267. (b) Xu, H. B.; Li, J.; Shi, L. X.; Chen, Z. N. *Dalton Trans.* **2011**, *40*, 5549. (c) Zhao, S.; Liu, X.; Feng, W.; Lü, X.; Wong, W. Y.; Wong, W. K. *Inorg. Chem. Commun.* **2012**, *20*, 41. (d) Bi, W. Y.; Lü, X. Q.; Chai, W. L.; Song, J. R.; Wong, W. Y.; Wong, W. K.; Jones, R. A. *J. Mol. Struct.* **2008**, *891*, 450. (e) Zhao, S.; Lü, X.; Hoy, A.; Wong, W. Y.; Wong, W. K.; Yang, X.; Jones, R. A. *Dalton Trans.* **2009**, 9595. (f) Feng, W.; Hui, Y.; Wei, T.; Lü, X.; Song, J.; Chen, Z.; Zhao, S.; Wong, W. K.; Jones, R. A. *Inorg. Chem. Commun.* **2011**, *14*, 75. (g) Muller, G.; Maupin, C. L.; Riehl, J. P.; Birkedal, H.; Piguet, C.; Bünzli, J. C. G. *Eur. J. Inorg. Chem.* **2003**, 4065. (h) Pasatoiu, T. D.; Tiseanu, C.; Madalan, A. M.; Jurca, B.; Duhayon, C. *Inorg. Chem.* **2011**, *50*, 5879.

(16) Sheldrick, G. M. *SHELXL-97: A Program for Crystal Structure Refinement*; University of Göttingen: Göttingen, Germany, 1997.

(17) *CrysAlis PRO*; Oxford Diffraction Ltd: Abingdon, Oxfordshire, U.K., 2010.

(18) Spek, A. L. *PLATON-94 (V-101094). A Multipurpose Crystallographic Tool*; University of Utrecht: Utrecht, The Netherlands, 1994.

(19) Clemente-Juan, J. M.; Coronado, E.; Gaita-Ariño, A. *Chem. Soc. Rev.* **2012**, *41*, 7464.

(20) (a) Yamashita, A.; Watanabe, A.; Akine, S.; Nabeshima, T.; Nakano, M.; Yamamura, T.; Kajiwara, T. *Angew. Chem., Int. Ed.* **2011**, *50*, 4016. (b) Feltham, H. L. C.; Klöwer, F.; Scott, A.; Cameron, A.; Larsen, D. S.; Lan, Y.; Tropiano, M.; Faulkner, S.; Powell, A. K.; Brooker, S. *Dalton Trans.* **2011**, *40*, 11425.

(21) (a) Baek, N. S.; Kim, Y. H.; Roh, S. G.; Kwuak, B. K.; Kim, H. K. *Adv. Funct. Mater.* **2006**, *16*, 1873. (b) Branchi, B.; Ceroni, P.; Balzani, V.; Klaerner, F. G.; Voegtle, F. *Chem.—Eur. J.* **2010**, *16*, 6048. (c) Lin, C. S.; Shi, X. S.; Li, J. R.; Wang, J. J.; Bu, X. H. *Cryst. Growth Des.* **2006**, *6*, 656. (d) Wang, J. J.; Lin, C. S.; Hu, T. L.; Chang, Z.; Li, C. Y.; Yan, L. F.; Chen, P. Q.; Bu, X. H.; Wu, Q.; Zhao, L. J. *Cryst. Eng. Commun.* **2008**, *10*, 681. (e) De Santis, G.; Fabbrizzi, L.; Licchelli, M.; Mangano, C.; Sacchi, D. *Inorg. Chem.* **1995**, *34*, 3581.

(22) Cao, D.-K.; Gu, Y.-W.; Feng, J. Q.; Caia, Z. S.; Ward, M. D. *Dalton Trans.* **2013**, *42*, 11436.

(23) (a) Klink, S. I.; Keizer, H.; van Veggel, F. C. J. M. *Angew. Chem., Int. Ed.* **2000**, *39*, 4319. (b) Imbert, D.; Cantuel, M.; Bünzli, J. C. G.; Bernardinelli, G.; Piguet, C. *J. Am. Chem. Soc.* **2003**, *125*, 15698. (c) Pope, S. J. A.; Coe, B.; Faulkner, S. *Chem. Commun.* **2004**, 1550.

(d) Shavaleev, N. M.; Accorsi, G.; Virgili, D.; Bell, Z. R.; Lazarides, T.; Calogero, G.; Armaroli, N.; Ward, M. D. *Inorg. Chem.* **2005**, *44*, 61.
(24) (a) Li, Q.-W.; Liu J.-L.; Jia, J.-H.; Leng, J.-D.; Lin, W.-Q.; Chen, Y.-C.; Tong, M.-L. (b) Liu, C.-S.; Du, M.; Sañudo, E. C.; Echevarria, J.; Hu, M.; Zhang, Q.; Zhou, L.-M; Fang, S.-M. *Dalton Trans.* **2011**, *40*, 9366. (c) Canaj, A. B.; Tzimopoulos, D. I.; Philippidis, A.; Kostakis, G. E.; Milios, C. J. *Inorg. Chem.* **2012**, *51*, 7451.